C-Terminal Domain of Insulin-like Growth Factor (IGF) Binding Protein 6: Conformational Exchange and Its Correlation with IGF-II Binding†

Shenggen Yao,*,‡ Stephen J. Headey,‡,§ David W. Keizer,‡ Leon A. Bach,§ and Raymond S. Norton*,‡

The Walter and Eliza Hall Institute of Medical Research, 1G Royal Parade, Parkville 3050, Australia, and Department of Medicine, University of Melbourne, Austin Hospital, Heidelberg 3084, Australia

Received March 18, 2004; Revised Manuscript Received June 11, 2004

ABSTRACT: Insulin-like growth factor binding proteins (IGFBPs) function as carriers and regulators of the insulin-like growth factors (IGF-I and -II). Within the family of six binding proteins, IGFBP-6 is unique in having a 20−100-fold higher affinity for IGF-II over IGF-I and appears to act primarily as an inhibitor of IGF-II actions. We have recently determined the solution structure of the C-terminal domain of IGFBP-6 (C-BP-6), which shows the presence of substantial flexible regions, including three loop regions. In this paper, we report results from ^{15}N relaxation measurements carried out in both the laboratory and rotating frames. Analysis of conventional ^{15}N relaxation data (R_1, R_2, and steady-state ^{15}N-{^{1}H} nuclear Overhauser effect) indicated that there was a considerable number of residues involved in conformational/chemical exchange. Measurements of off-resonance ^{15}N $R_{1\rho}$ in the rotating frame and ^{15}N relaxation dispersion using an in- and antiphase coherence-averaged Carr−Purcell−Meiboom−Gill sequence were thus carried out to gain further insight into the solution dynamics of C-BP-6. Although the off-resonance ^{15}N relaxation data showed no clear evidence for residues undergoing microsecond motion, the ^{15}N relaxation dispersion data allowed us to identify 15 residues that clearly exhibit submilli- to millisecond motion. A good correlation was observed between residues exhibiting motion at submilli- to millisecond time scales and those affected by IGF-II binding, as identified through the perturbation of nuclear magnetic resonance (NMR) spectra of C-BP-6 following IGF-II addition. A complete NMR relaxation study of C-BP-6 dynamics in complex with IGF-II was hampered by peak broadening and disappearance of C-BP-6 in the presence of IGF-II. Nonetheless, current results strongly suggest possible conformation switching or population shifting between pre-existing conformations in C-BP-6 upon binding to IGF-II.

Insulin-like growth factors (IGF-I and -II)[1] are essential for pre- and postnatal physiological growth and have critical roles in normal mammalian development (*1*). IGF-I mediates most of the growth-promoting effects of the growth hormone, whereas IGF-II is largely growth-hormone-independent. Disregulation of the IGF system has been implicated in a wide range of disease processes, including various cancers, atherosclerosis, neuromuscular disease, and diabetic complications (*2*). The actions of IGFs are regulated by a family of six structurally related, high-affinity IGF binding proteins (IGFBPs 1−6). When the IGFBPs bind to the circulating IGFs, they regulate the passage of IGFs into tissues and greatly prolong the circulating half-lives of IGFs. Within the IGFBP family, IGFBP-6 is distinct mainly in its marked preferential binding affinity for IGF-II over IGF-I, and it is essentially an inhibitory IGFBP (*3*).

All of the IGFBPs consist of three distinct domains of approximately equal size. The N- and C-terminal domains, which contain the IGF-binding sites, are cysteine-rich as well as highly homologous in amino acid sequence among the six family members. In contrast, the central-linker domains, which are thought not to contain IGF-binding sites, are more divergent in sequence (*4*). The 3D structures of full-length IGFBPs have not yet been determined. The only structural information available is for residues 40−92 of the N-domain of IGFBP-5 (mini-IGFBP-5), alone (*5*) and in complex with IGF-I (*6*).We have recently solved the 3D structure of the C-terminal domain of IGFBP-6 (C-BP-6) using NMR spectroscopy (Figure 1; Headey, S. J., Keizer, D. W., Yao, S., Kantharidis, P., Bach, L. A., and Norton, R. S. (2004) C-terminal domain of insulin-like growth factor binding protein-6: structure and interaction with insulin-like growth factor-II. *Molecular Endocrinology*, accepted for publication.). The principal features of the C-BP-6 structure include a four-turn α helix at the beginning of the C domain (Pro162-Thr176), a type-I β turn (Asp191-Gly194), and a three-stranded antiparallel β sheet (Leu185-Asp191, Arg199-Ser204, and Cys212-Val215), which is separated from the α helix by a loop region. The C-terminal half of C-BP-6 features a second, moderately well-ordered, loop between

† This work was supported in part by a grant (114156) from the National Health and Medical Research Council (NHMRC) of Australia. S.J.H. is a recipient of an NHMRC Dora Lush Postgraduate Research Scholarship.

* To whom correspondence should be addressed. E-mail: syao@wehi.edu.au (S.Y.); ray.norton@wehi.edu.au (R.S.N.).

‡ The Walter and Eliza Hall Institute of Medical Research.

§ University of Melbourne.

[1] Abbreviations: IGF, insulin-like growth factor; IGFBP, insulin-like growth factor binding protein; C-BP-6, C-terminal domain of insulin-like growth factor binding protein 6; CPMG, Carr−Purcell−Meiboom−Gill; CSA, chemical-shift anisotropy; HSQC, heteronuclear single-quantum coherence; NMR, nuclear magnetic resonance; NOE, nuclear Overhauser effect; SD, standard deviation.

10.1021/bi049456+ CCC: $27.50
Published on Web 08/11/2004

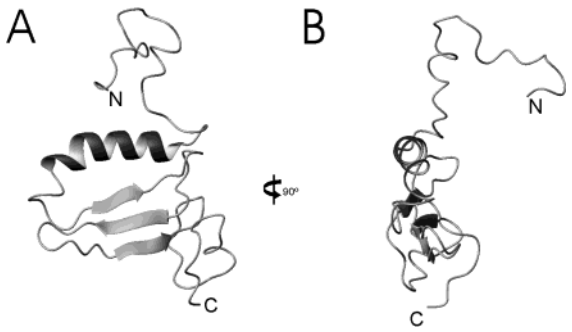

FIGURE 1: (A) Ribbon diagram of the solution structure of C-BP-6 (161−240) including a 27-residue leader sequence, showing the influence of the leader sequence on the shape of molecule and thus the global reorientation behavior. Although the N-terminal hexa-His tag is poorly defined in the structure because of a lack of restraints in the structure calculation, its moderate ^{15}N NOE values (Figure 3C) suggest that it may actually have some contact with the C-BP-6. (B) 90° rotation around the vertical axis of A. This figure was prepared using MOLMOL (*45*).

the second and the third strands. A third, highly disordered, loop and unstructured tail are located after the second distorted type-I β turn, beginning from Asp216.

Nuclear magnetic resonance (NMR) relaxation measurements provide a means of characterizing the protein solution dynamics over a broad range of time scales. Experimental procedures for measuring ^{15}N relaxation parameters [R_1, R_2, and steady-state ^{15}N-{^{1}H} nuclear Overhauser effect (NOE)] as well as protocols for data analysis using Modelfree formalism are well-established for the study of protein backbone dynamics at pico- to nanosecond time scales (*7*, *8*). NMR relaxation methods have been applied to numerous protein systems, including mini-IGFBP-5, both in its free form and in complex with IGF-I, revealing changes in dynamics on the pico- to nanosecond time scales for residues involved in the binding interaction (*9*). Recently, there has been increasing evidence that protein dynamics in solution, particularly on the millisecond time scale, may correlate closely with protein−protein interactions at the structural level (*10*, *11*). This is significant because one of the mechanisms behind protein function and protein−protein interaction is conformational exchange, which typically occurs at the submilli- to millisecond time scales (*12*). In our structural study of C-BP-6 by NMR, it was noticed that a number of residues (located within the second β strand and second loop as well as in close proximity to the first loop) gave rise to dual peaks in the ^{15}N-^{1}H heteronuclear single-quantum coherence (HSQC) spectrum, possibly because of slow chemical/conformational exchange. In this paper, we present the results of a comprehensive ^{15}N relaxation study of C-BP-6, with measurements carried out in both the laboratory and rotating frames, in an attempt to gain further insight into not only its backbone dynamics on pico- to nanosecond time scales, but also into those residues undergoing micro- to millisecond time scale motion and their potential correlation with IGF-II binding.

EXPERIMENTAL PROCEDURES

Sample Preparation. The cloning, expression, and purification of C-BP-6 used for structural and dynamics studies have been described previously (*13*). The C-BP-6 construct used in the present study comprised residues 161−240 of IGFBP-6 and a pProEx HTb vector (Life Technologies) leader sequence of 27 residues (numbered −27 to −1 here). The uniformly ^{15}N-labeled sample used for NMR relaxation measurements contained 1 mM protein in 10 mM sodium acetate (pH 4.5) and 0.02% (w/v) sodium azide, in 95% H_2O/5% ^2H_2O.

Relaxation Measurements. All relaxation measurements were carried out at 25 °C on a Bruker DRX600 spectrometer using a triple-resonance probe equipped with triple-axis gradients. Spectral widths of 7185 and 1700 Hz for ^{1}H and ^{15}N, respectively, were used throughout the measurements. Laboratory-frame ^{15}N relaxation rates (R_1, R_2, and steady-state ^{15}N-{^{1}H}NOE) were measured using pulse sequences similar to those published previously (*14*). A matrix size of 2048 × 180 and 32 scans per t_1 increment were used. A total of 14 relaxation durations, including 2 duplicated durations, ranging from 10 ms to 1.5 s for R_1 and 15.4 to 540 ms for R_2 were used. The recycle times used were 2.2 s for R_1 and R_2 and 3.2 s for the steady-state ^{15}N-{^{1}H}NOE, respectively. All data were recorded in an interleaved manner.

The off-resonance rotating-frame ^{15}N relaxation rate ($R_{1\rho}$) was measured using a sequence modified from that used for the R_1 measurement, in which a radio frequency spin-lock pulse with a field strength of ω_1 and an offset of $\Delta\Omega$ from the center of the ^{15}N carrier frequency was applied during the relaxation period (*15*, *16*). The rotation of nuclear spin magnetization toward and backward from the appropriate effective field was achieved by an adiabatic half-passage pulse of 4-ms duration (*17*). Suppression of cross correlation between dipole−dipole and CSA relaxation during the relaxation period was achieved by ^{1}H spin inversion every 5 ms (*14*). A matrix size of 2048 × 128, 16 scans per t_1 increment, and a recycle time of 2.2 s were used. The spin-lock field strength employed was 1650 Hz, and the off-resonance radio frequency field was placed at −8000, −6000, −4000, −3000, −2000, −1400, −1000, −600, −300, and 0 Hz from the center of the ^{15}N carrier frequency. Eight relaxation durations of 10, 20, 30, 50, 70, 100, 150, and 200 ms were recorded for all off-resonance frequencies.

In- and antiphase coherence-averaged ^{15}N transverse relaxation rates (R_2^{app}) as a function of an extended Carr−Purcell−Meiboom−Gill (CPMG) delay were measured using a pulse sequence modified from that used for the R_2 measurement, in which the relaxation period was replaced with a relaxation-compensated CPMG segment (*18*, *19*). Eight 3D data sets with B_1 field strengths, ν_{CPMG}, of 50, 100, 125, 167, 250, 333, 500, and 1000 Hz (corresponding to delays, between the center of two consecutive 180° pulses in the CPMG segment, of 10, 5, 4, 3, 2, 1.5, 1, and 0.5 ms, respectively) at eight relaxation durations ranging from 2 to 320 ms were recorded. A matrix size of 2048 × 128, 16 scans per t_1 increment, and a recycle time of 2.2 s were used.

Analysis of Relaxation Data. All spectra were processed using XWINNMR (version 3.1, Bruker Biospin) and analyzed with XEASY version 1.3 (*20*). ^{15}N relaxation rates R_2, $R_{1\rho}$, and R_2^{app} were obtained by fitting peak intensities at a series of relaxation durations to a two-parameter single-exponential-decay curve using curvefit (A. G. Palmer, Columbia University), whereas the fitting of a three-parameter exponential-decay curve was used for R_1. Errors of the relaxation rates were determined by curvefit using a Monte Carlo simulation. The steady-state ^{15}N-{^{1}H}NOE

values were calculated from peak intensity ratios obtained from spectra acquired in the presence and absence of proton saturation. The uncertainties of peak intensities for ^{15}N R_1, R_2, $R_{1\rho}$, and R_2^{app} measurements were derived from those duplicated spectra, whereas corresponding uncertainties for the peaks of steady-state ^{15}N-{^{1}H}NOE spectra were estimated from the background noise of the spectra (*14*).

Modelfree Analysis. Initial estimation of the global reorientation time of C-BP-6 was obtained by analysis of R_2/R_1 ratios from residues satisfying the criteria of both steady-state ^{15}N-{^{1}H}NOE $\geq$ 0.6 and $|T_1/T_2 - \langle T_1/T_2\rangle| \leq$ standard deviation (SD) (*21*), which assumes the global reorientation to be isotropic. The ratio of three principal moments of the inertial tensor of C-BP-6 was obtained from its solution structure using pdbinertial (A. G. Palmer, Columbia University). The rotational-diffusion tensor of the C-BP-6 was obtained from the ratios of R_1 and R_2 values of selected residues, which satisfy both steady-state ^{15}N-{^{1}H}NOE $\geq$ 0.65 and $|T_1/\langle T_1\rangle - T_2/\langle T_2\rangle| \leq$ 1.5 SD (*22*) using r2r1_diffusion (A. G. Palmer, Columbia University) and TENSOR2 (*23*). Residues exhibiting slow submillisecond motion, as identified from relaxation dispersion studies (see below), were also excluded from determination of its global rotational-diffusion parameters. Modelfree analysis was carried out using Modelfree (version 4.0, A. G. Palmer, Columbia University) and TENSOR2 (*23*), but only the dynamics parameters from Modelfree are reported here, unless otherwise indicated. An N−H bond length of 1.02 Å and an amide ^{15}N chemical anisotropy of −170 ppm were used for the analysis. After a model for the global reorientation of C-BP-6 was determined, ^{15}N relaxation data of R_1, R_2, and steady-state ^{15}N-{^{1}H}NOE were fitted to one of five combinations of Modelfree parameters, similar to the model selection approach (*24*).

Fitting of Nano- to Microsecond Dynamics Parameters. The relaxation rate measured in the presence of a transverse spin-locking field applied off-resonance is given by (*16*, *25*) with

$$R_{1\rho} = R_1 \cos^2(\theta) + (R_2 + R_{ex}) \sin^2(\theta) \quad (1)$$

$$R_{ex} = (\omega_A - \omega_B)^2 p_A p_B (\tau_{ex}/(1 + \tau^2{}_{ex}\omega^2{}_{eff})) \quad (2)$$

where ω_A and p_A, and ω_B and p_B are resonance frequencies and populations for the nuclear spin in sites A and B, respectively; τ_{ex} is the time constant for the exchange process; $\omega_{eff} = (\Delta\omega^2 + \omega_1{}^2)^{1/2}$ is the strength of the effective field, with ω_1 being the strength of the spin-locking field applied at an off-resonance frequency $\Delta\omega$ with respect to the spin-resonant frequency. The angle $\theta = \tan^{-1}(\omega_1/\Delta\omega)$ is the tilt angle of the effective field in relation to the static magnetic field. For a given offset of the spin-locking field ($\Delta\Omega$), $\Delta\omega$ is residue-dependent. The apparent transverse relaxation rate, $R_2' = R_2 + R_{ex}$, at any given ω_{eff} values can be calculated from experimentally measured $R_{1\rho}$ values using eq 1. Resultant R_2' values were then fitted as a function of ω_{eff} according to eqs 1 and 2.

The apparent transverse relaxation rate, R_2^{app}, obtained from an in- and antiphase coherence-averaged CPMG sequence is given by (18)

$$R_2{}^{app} = R_2{}^{ave} + R_{ex} \quad (3)$$

where R_2^{ave} is the transverse relaxation rate averaged over the in- and antiphase coherences and R_{ex} is the rate constant arising from chemical or conformational exchange between sites. For two exchanging sites,

$$R_{ex} = (\omega_A - \omega_B)^2 p_A p_B \tau_{ex}[1 - 8\tau_{ex}\nu_{CPMG} \tanh(1/(8\nu_{CPMG}\tau_{ex}))] \quad (4)$$

where ω_A, p_A, ω_B, p_B, and τ_{ex} have the same meanings as in eq 2. ν_{CPMG} is defined as $1/(4\tau_{CPMG})$, with $2\tau_{CPMG}$ being the separation between the center of two successive 180° pulses in the CPMG segment. The experimental R_2^{app} values were fitted as a function of ν_{CPMG} according to eqs 3 and 4.

Amide Exchange. Slow amide exchange of C-BP-6 residues was detected from the persistence of their cross peaks in the ^{1}H-^{15}N HSQC spectra at 10 °C after dissolving in 10 mM sodium acetate (pH 4.5) and 0.02% (w/v) sodium azide in 100% ^2H_2O. A lower temperature was chosen in this study to prolong the exchange process and therefore facilitate the measurements. Rapid amide exchange was detected using CLEANEX sequence with mixing times of 26 and 52 ms, respectively (*26*).

Hydrodynamic Calculation and Translational-Diffusion Measurements. Hydrodynamic parameters of C-BP-6 were also estimated from its 3D coordinates (closest to the average of the family of 20 structures, PDB 1RMJ) (*27*) using HYDRONMR based on atomic-bead modeling (*28*). A value of 0.8921×10^{-3} Nm^{-2} s, the viscosity of water at 25 °C, was used in the computation. Translational-diffusion-coefficient measurements were performed on the same C-BP-6 sample and under the same experimental conditions as for relaxation measurements. Details of the pulse sequence used, the calibration of pulsed-field gradient strength, and the data analysis have been described previously (*29*). Briefly, a series of 12 diffusion-weighted spectra was recorded in a 2D manner using gradient pulses of 6-ms duration, a separation of 46.8 ms, and gradient strengths ranging from 3.4 to 36.5 G cm^{-1}.

RESULTS

^{15}N Relaxation Data. Representative ^{15}N relaxation decay curves are shown in Figure 2. A summary of backbone ^{15}N R_1, R_2, R_2' (calculated using eq 1 from $R_{1\rho}$ acquired with an offset $\Delta\Omega = 0.0$ Hz), and ^{15}N-{^{1}H} steady-state NOE values for C-BP-6 is given in Figure 3. With the exception of a few residues (Figure 3B), R_2' values appear in general slightly faster than those from conventional CPMG methods, reflecting the fact that the off-resonance effect in the conventional CPMG sequence results in a slightly underestimated R_2 (*30*). After the residues heavily overlapped in the spectra were excluded, all three R_1, R_2, and steady-state ^{15}N-{^{1}H}NOE values were measured for 79 residues, giving averaged values of 1.56 ± 0.18, 10.35 ± 3.17, and 0.60 ± 0.28 s^{-1}, respectively. Of these 79 residues, 68 residues arise from the native C-terminal domain, 161−240 of IGFBP-6, and 11 from the leader sequence (C-BP-6 contains six prolines).

Amide Exchange. Most amide protons of C-BP-6 were found to be in fairly rapid exchange with water. Only a few amides from residues located within and near the type-I β turn (Asp191-Gly194) were detected in the ^{15}N-^{1}H HSQC

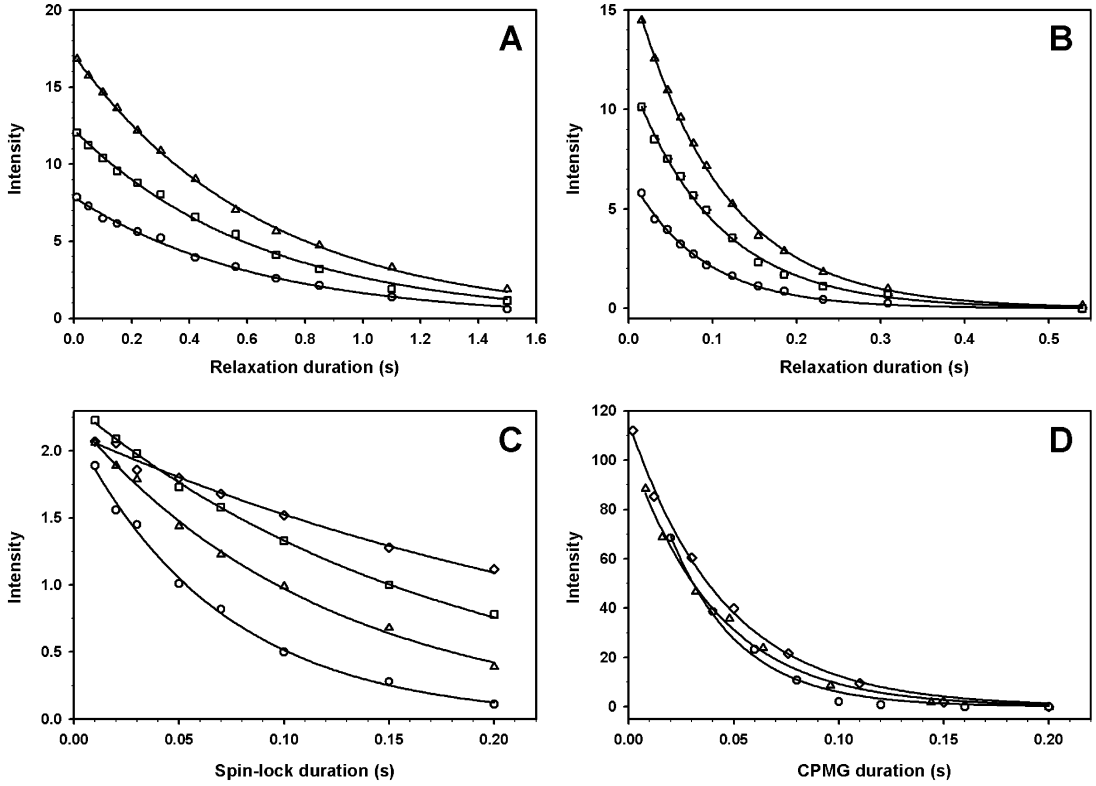

FIGURE 2: Representative ^{15}N relaxation decay curves of C-BP-6. (A) R_1 and (B) R_2 for residues His166 (○), Val178 (△), and Ser221 (□). (C) $R_{1\rho}$ of His166 at off-resonance frequencies, $\Delta\Omega$, of 0 Hz (○), 1400 Hz (△), 3000 Hz, (□), and 8000 Hz (◇). (D) R_2^{app} of Asp216 at CPMG field strengths of 100 Hz (○), 250 Hz (△), and 1000 Hz (◇).

spectra after being dissolved in acetate buffer in 100% ^2H_2O for 4 h. The CLEANEX experiments revealed that the amide protons in most rapid exchange with the solvent were located in the disordered first and third loops, the distal half of the second loop, and the C-terminal tail. Several amides on the solvent-exposed side of the α helix also showed relatively rapid exchange with ^2H_2O, including Arg165, Ser169, and Gln172.

Overall Translational and Rotational Motion of C-BP-6. The translational-diffusion coefficient of the C-BP-6 was measured to be $1.20 \pm 0.05 \times 10^{-10}$ m^2 s^{-1} at 25 °C. The result was reproducible over measurements carried out several months apart as well as from several samples used in the structural studies.

Of the 79 residues whose R_1, R_2, and steady-state ^{15}N-{^1H}NOE values were measured, 29 satisfy the criteria of steady-state ^{15}N-{^1H}NOE ≥ 0.6 and $|T_1/T_2 - \langle T_1/T_2\rangle| \leq$ SD, indicating that those nuclear spins are unlikely to participate in either slow internal motion or chemical/conformational exchange processes. An isotropic global correlation time of 8.3 ± 0.5 ns was thus obtained (*21*, *31*). On the basis of the structure of C-BP-6 (in the presence of the leader sequence) (Figure 1), the principal moments of its inertia tensor were calculated to be 1:0.86:0.43. Parameters of the axially symmetric rotational-diffusion tensor were obtained using the R_1 and R_2 values of 38 residues, which satisfy both steady-state ^{15}N-{^1H}NOE ≥ 0.65 and $|T_1/\langle T_1\rangle - T_2/\langle T_2\rangle| \leq 1.5$ SD (22). r2r1_diffusion (A. G. Palmer, Columbia University) resulted in a prolate model with $D_\parallel/D_\perp = 1.4 \pm 0.1$. TENSOR2 (*23*), on the other hand, revealed two equally significant minima representing prolate and oblate approximations ($D_\parallel = 2.32 \pm 0.12 \times 10^7$ s^{-1}, $D_\perp = 1.89 \pm 0.02 \times 10^7$ s^{-1} and $D_\parallel = 1.72 \pm 0.08 \times 10^7$ s^{-1}, $D_\perp = 2.19 \pm 0.05 \times 10^7$ s^{-1}, respectively), while a fully anisotropic model gave no statistically significant improvement in the target function, as expected in such a case (*32*). Hydrodynamics calculations based on the closest to the average of a family of 20 structures (PDB 1RMJ) resulted in a translational-diffusion coefficient of 1.11×10^{-10} m^2 s^{-1} and principal components of the rotational-diffusion tensor of 2.02, 1.36, and 1.26×10^7 s^{-1}, respectively. This gives an anisotropy $D_\parallel/D_\perp = 1.54$, which is in reasonable agreement with those derived from the ^{15}N relaxation data. Final values for the rotational-diffusion anisotropy $D_\parallel/D_\perp$ and effective correlation time $(4D_\perp + 2D_\parallel)^{-1}$ of 1.5 and 8.0 ns, respectively, were obtained for the global rotational-diffusion tensor of C-BP-6 after optimization using the combination of Modelfree parameters for each residue (see below).

Modelfree Parameters. Using an axially symmetric model for the global rotational reorientation motion of C-BP-6, Modelfree parameters (S^2, τ_f/τ_s, and R_{ex}) of individual residues were obtained from fits of the ^{15}N relaxation data (R_1, R_2, and steady-state ^{15}N-{^1H}NOE) using the model selection approach. A total of 65 residues, including 8 from the leader sequence, were fitted successfully to one of the five models as summarized in Figure 4. Numbers of residues fitted satisfactorily to each combination of Modelfree parameters were 21 (S^2), 12 (S^2 and τ_f), 4 (S^2 and R_{ex}), 7 (S^2, τ_f, and R_{ex}), and 21 (S^2_f, S^2_s, and τ_s), respectively. The averaged S^2 value over those 65 residues is 0.76 ± 0.23, and the corresponding value for C-BP-6 (161−240) is 0.77 ± 0.24. Averaged values of S^2 for the four-turn α helix (Pro162-Thr176), three stranded antiparallel β sheet (β1 = Leu185-Asp191, β2 = Arg199-Ser204, and β3 = Cys212-Val215), the first loop region (Glu177-Thr184), the second loop region (Gln205-Pro211), and the highly disordered third

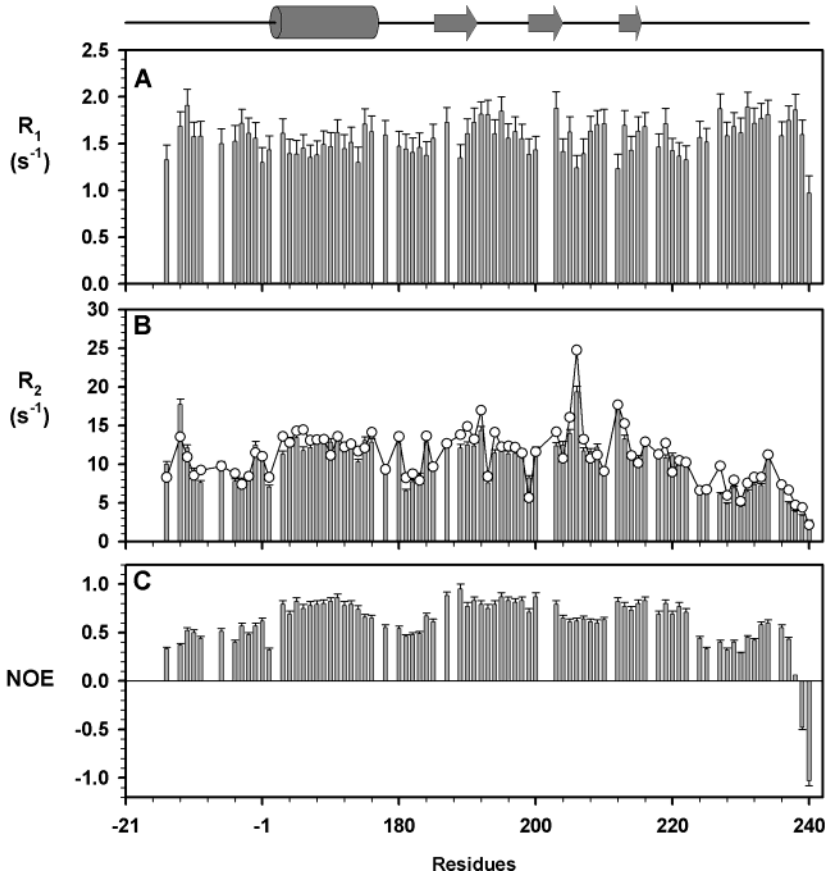

FIGURE 3: Summary of backbone ^{15}N relaxation parameters (A) R_1, (B) R_2, and (C) steady-state ^{15}N-{^1H}NOE for C-BP-6, measured at 25 °C and ^{15}N frequency of 60.81 MHz. R_2' values calculated from $R_{1\rho}$ after correction for the off-resonance effect are also shown in B (○). The $R_{1\rho}$ data recorded at the offset $\Delta\Omega = 0.0$ Hz were used in the calculation. Elevated R_2 values for residues Thr(−13), Gly206, and Cys212 are clearly evident in B.

loop region plus the C-terminal tail are 0.94 ± 0.06, 0.90 ± 0.11, 0.71 ± 0.13, 0.78 ± 0.08, and 0.38 ± 0.14, respectively.

Slow Motional Parameters from Direct Measurements. Representative ^{15}N transverse relaxation rates, R_2', as calculated from rotating frame $R_{1\rho}$ data at a number of effective field strengths, and R_2^{app} values at a series of CPMG field strengths (relaxation dispersion curve) are shown in Figure 5. For all 79 residues where the rotating frame $R_{1\rho}$ values were measured, no decline in R_2' as a function of the effective field strength was evident. All of the data appeared to be scattered around their "mean" values (Figure 5A). Attempts to fit the data to eqs 1 and 2, therefore, were unsuccessful. In contrast, from experimentally measured relaxation dispersion data (coherence-averaged R_2^{app} as a function of CPMG field strengths), 20 residues were fitted successfully to eqs 3 and 4 with τ_{ex} values ranging from 0.52 to 2.4 ms, as summarized in Table 1.

DISCUSSION

Conventional ^{15}N relaxation measurements (R_1, R_2, and steady-state ^{15}N-{^1H}NOE) provide information on protein backbone mobility at pico- to nanosecond time scales as well as slow motion on the millisecond time scale. The latter is achieved through Modelfree analysis of ^{15}N R_1, R_2, and steady-state ^{15}N-{^1H}NOE data with the inclusion of an additional term, R_{ex}, to account for contributions from chemical/conformational exchange. Studies of protein motion at micro- to millisecond time scales, which may provide potentially valuable information in understanding protein function and protein−protein interactions, may also be achieved through direct NMR relaxation measurements using a number of alternative methods, including analysis of backbone ^{15}N relaxation parameters measured at several B_0 fields (*33*), off-resonance ^{15}N $R_{1\rho}$ in the rotating frame (*15*, *16*), and ^{15}N relaxation dispersion data using an in- and antiphase coherence-averaged CPMG sequence (*18*, *19*). In the present study, we have carried out ^{15}N relaxation measurements of C-BP-6 in both the laboratory and rotating frames. Although the off-resonance ^{15}N relaxation data fail to detect any residues undergoing microsecond motion, a substantial number of residues exhibit motion at submilli- to millisecond time scales, as identified by Modelfree analysis and ^{15}N relaxation dispersion data obtained using the coherence-averaged CPMG method. These residues correlate well with those affected by IGF-II binding, as identified through the perturbation of NMR spectra upon IGF-II addition (*34*) (Figure 6).

Probing Microsecond Motions of C-BP-6 via Rotating Frame Off-Resonance $R_{1\rho}$ Measurements. Rotating frame off-resonance experiments have been applied successfully in several protein systems recently (*35*, *36*). In the present study, however, there was no evident dependence of $R_{1\rho}$ on the effective field strengths applied, as would have been expected for residues undergoing conformational exchange at time scales ranging from micro- to submillisecond. One possible

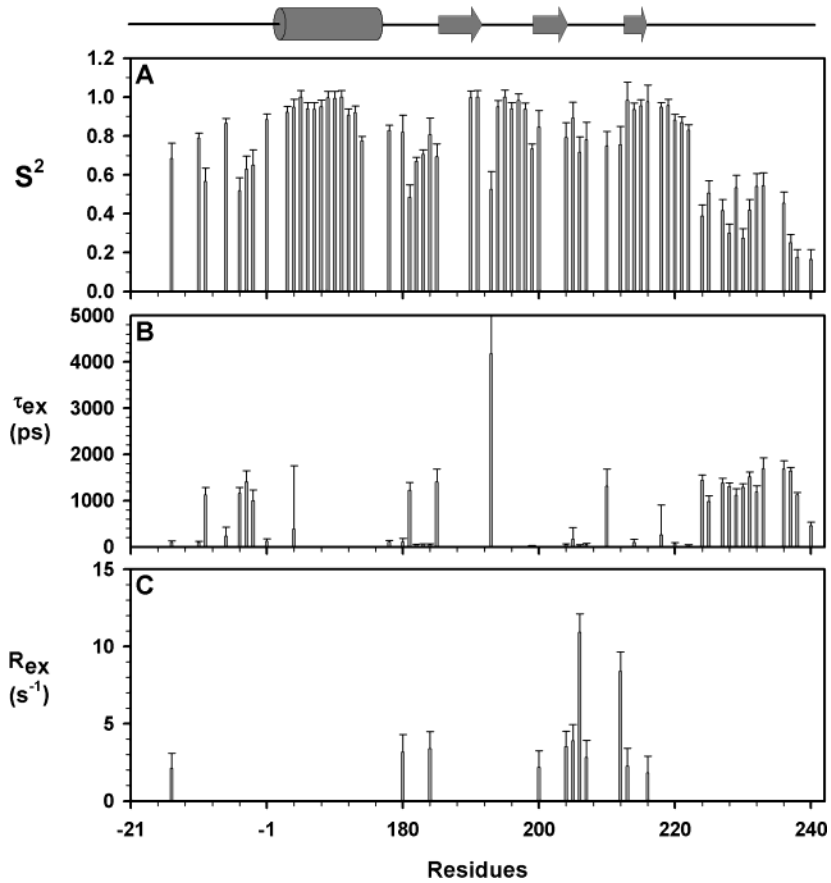

FIGURE 4: Summary of Modelfree parameters for C-BP-6 obtained using the extended spectral density function and the model selection approach. An axially symmetric rotational-diffusion tensor was used to describe the global rotational motion of C-BP-6. (A) Order parameter, S^2 ($= S^2_f \times S^2_s$). (B) Effective internal correlation time, τ_e (τ_f or τ_s). (C) Apparent chemical/conformational exchange contribution R_{ex} to the transverse relaxation rate R_2.

reason is the relatively large experimental uncertainties associated with the transverse relaxation measurements in the rotating frame, as reported previously (*9*). Off-resonance $R_{1\rho}$ measurements require the application of a spin-lock pulse during the relaxation period, which limits the longest relaxation duration that can be used because of sample heating. A longer relaxation duration, however, is desirable in certain cases to allow the magnetization to decay sufficiently, in particular when θ approaches 0° and $R_{1\rho}$ approaches R_1. Typically, a maximum relaxation duration of around 200 ms can be used before sample heating becomes noticeable, which corresponds to an approximately 35% decay of the magnetization only at $\theta = 15°$ for spins with ^{15}N relaxation rates of $R_1 = 1.67$ and $R_2 = 10$ s^{-1}. Clearly, this error will be more pronounced for spins undergoing conformational/chemical exchange, which have a shorter apparent R_2 and thus a poor signal/noise ratio. In addition, the effects of spin-lock B_1 field inhomogeneity are more severe at larger offsets. As a consequence, the $R_{1\rho}$ values measured at small tilt angles of the effective field are likely to incur larger errors. In the present study, elevated R'_2 values were observed for those calculated from $R_{1\rho}$ data recorded with offsets of −6000 and −8000 Hz.

Dynamics of C-BP-6 from Modelfree Analysis. An average S^2 value of 0.78 indicates that the backbone of C-BP-6 is fairly mobile, while higher S^2 values across the α helix and β strands, 0.94 and 0.89, respectively, indicate less flexibility compared to the loop regions. To satisfactorily fit the Modelfree formalism, a R_{ex} term, which accounts for the contribution of additional chemical/conformational exchange, was required for 11 residues (Figure 4C). Unlike other protein systems, where residues exhibiting conformational/chemical exchange were scattered across the sequence (*37*), in C-BP-6, they form a small cluster at the end of the second β strand and the beginning of the second loop of C-BP-6, involving residues Ser204, Gln205, Gly206, and Gln207, along with others in close proximity, such as Cys212, Trp213, and Asp216. The observation that a considerable number of residues in this region undergo conformational exchange at the submillisecond time scale is not too surprising because it might arise from isomerization of the disulfide bridge between Cys201 and Cys212.

Conformation Exchange of C-BP-6 from Modelfree Analysis and Coherence-Averaged CPMG Measurements. Only 3 residues of the 11 which exhibit millisecond motion from Modelfree analysis coincide with residues showing slow motion according to the coherence-averaged CPMG method (Table 1). This is not too surprising because these two methods are complementary to each other in terms of the motional time scales that they detect. Furthermore, protein conformational/chemical exchange detected by the Modelfree analysis will, to some extent, be influenced by the predetermined global rotational-diffusion parameters (*38*). The accuracy of estimating global rotational-diffusion parameters remains limited because of a lack of independent measures of molecular rotational diffusion in solution. This is particularly true for relatively flexible molecules, where only a limited number of residues satisfy the criteria for use in the

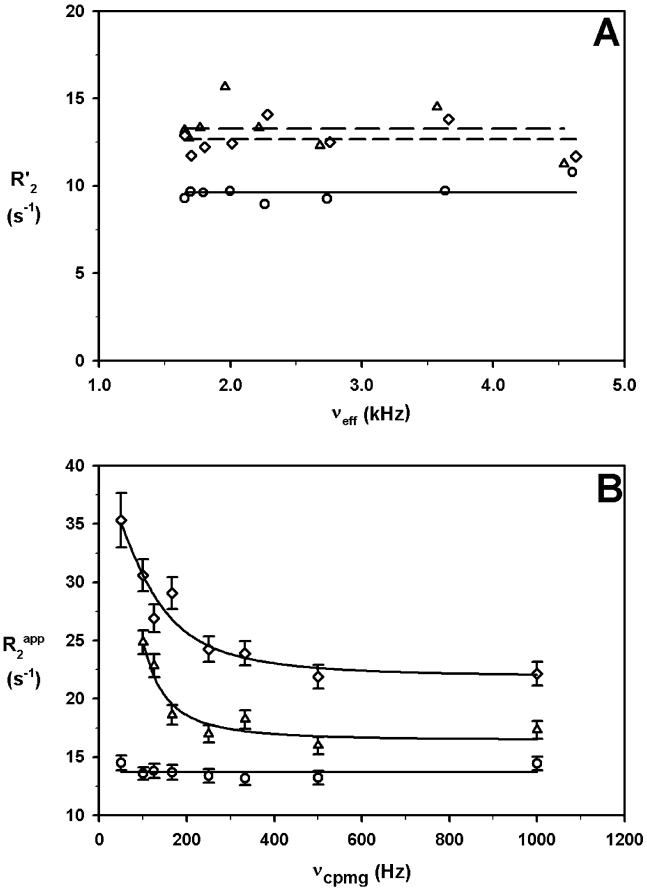

FIGURE 5: Transverse relaxation rate R_2' calculated from $R_{1\rho}$ values as a function of the effective field strengths in the rotating frame (A) and apparent transverse relaxation rate R_2^{app} as a function of CPMG field strengths (B) for residues Val178 (○), Gln207 (△), and Asp216 (◇), respectively. In A, the lines are drawn at the averaged R_2' values across the range of the effective field for residues Val178 (—), Gln207 (— —), and Asp216 (- - -). In B, the line is drawn for residue Val178 at its average R_2^{app} value, whereas for residues Gln207 and Asp216, the lines represent the best fit to eqs 3 and 4.

estimation of global rotational behavior. As a consequence, the resultant global rotational parameters may not reflect the full picture of the global anisotropy of the molecule (*39*). On the other hand, while conformational exchange determined from the coherence-averaged CPMG method is not affected by how accurately the global rotational parameters of a molecule are determined, residues undergoing relative slow conformational/chemical exchange and therefore exhibiting elevated R_2 values may not be measurable at all in the coherence-averaged CPMG method because of the extended CPMG interval as well as the inclusion of an antiphase magnetization evolution period (*18*, *40*). This was the case for residues Thr(−13), Gly206, and Cys212 in the present study. It is also worth noting that, while the amide exchange study indicated that most amides of C-BP-6 were in relatively fast exchange with water, including residues located on the solvent-exposed side of the α helix, several residues (Cys163, Arg165, and Leu171; see Table 1) within the α helix of C-BP-6 also exhibited conformational exchange.

Implications of C-BP-6 Conformational Exchange for IGF-II Binding. Residues of C-BP-6 involved in IGF-II binding have been identified recently through the perturbation of

Table 1: Dynamics Parameters of C-BP-6 Residues Undergoing Relatively Fast Conformational/Chemical Exchange from ^{15}N Relaxation Data Measured Using the Coherence-Averaged CPMG Method

residues[a]	τ_{ex} (ms)	$\Phi_{ex}\tau_{ex}$ (s^{-1})[b]	R_2^{ave} (s^{-1})
Gly161	1.20 ± 0.20	11.6 ± 0.9	14.4 ± 0.4
Cys163	0.97 ± 0.46	5.3 ± 1.0	18.1 ± 0.8
Arg165[c]	1.20 ± 0.50	6.8 ± 1.7	22.7 ± 0.7
Leu171	1.00 ± 0.50	15.2 ± 4.0	20.6 ± 1.6
Gln175[c]	0.50 ± 0.10	9.2 ± 0.8	18.8 ± 0.7
Cys190[d]	0.58 ± 0.24	9.1 ± 1.5	21.5 ± 1.2
Arg193[c]	1.20 ± 0.20	3.6 ± 0.4	10.5 ± 0.2
Gly194[c]	2.10 ± 0.80	17.1 ± 4.5	20.3 ± 1.0
Phe195	2.40 ± 0.30	19.7 ± 2.4	20.6 ± 0.3
Ser203[d]	0.52 ± 0.15	7.9 ± 0.8	24.9 ± 0.7
Gln207[e]	0.93 ± 0.60	9.8 ± 3.0	16.1 ± 1.7
Arg209[d]	1.15 ± 0.49	17.6 ± 4.2	20.6 ± 1.9
Gly210[d]	0.89 ± 0.55	24.4 ± 8.6	15.8 ± 3.0
Asp216[e]	1.40 ± 0.40	18.1 ± 2.9	21.9 ± 1.0
Ser221	1.75 ± 0.30	8.0 ± 1.0	15.8 ± 0.2

[a] Motion at the millisecond time scale was also observed for several residues from the leader sequence [Ile(−15), Thr(−12), Met(−3), Gly(−2), and Ser(−1)]. [b] $\Phi_{ex} = (\omega_A - \omega_B)^2 p_A p_B$. [c] Residues showing a significant increase in R_2 upon IGF-II binding. [d] Residues with ^1H-^{15}N cross peaks, which disappeared in HSQC spectra upon addition of IGF-II. [e] Residues where millisecond motion arising from conformational/chemical exchange was also indicated from the Modelfree analysis.

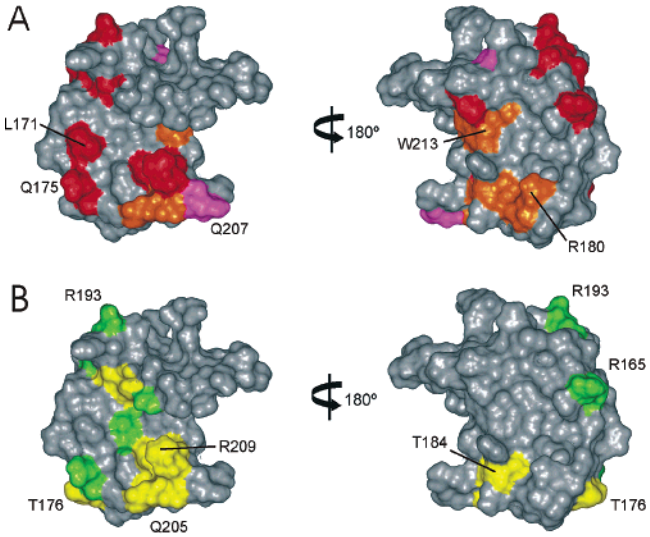

FIGURE 6: Surface diagrams of C-BP-6 (161−240) showing residues exhibiting conformational exchange (A) and residues affected by IGF-II binding (B). Color schemes: (A) red, identified by coherence-averaged CPMG sequence; orange, identified by Modelfree analysis; and pink, identified by both; (B) yellow, identified by ^1H-^{15}N cross peaks, which disappeared in HSQC spectra upon addition of IGF-II; and green, identified by those showing significant increases in R_2 at a C-BP-6/IGF-II ratio of 1:1. This figure was prepared using InsightII (Accelrys, San Diego, CA).

NMR spectra upon IGF-II addition (*34*). Figure 6 shows surface diagrams of C-BP-6 highlighting residues exhibiting conformational exchange and those affected upon IGF-II binding highlighted. Clearly, there is a good correlation between residues exhibiting motion at submilli- to millisecond time scales and those involved in IGF-II binding. Measurements of complete relaxation parameters of C-BP-6 in complex with IGF-II, as described here for C-BP-6 in free form, were not possible because many peaks disappeared upon addition of IGF-II into ^{15}N-labeled C-BP-6. This was still the case even after an IGF-II/C-BP-6 ratio of 2:1 was

reached, although peaks were restored when the pH was reduced to 3.0, where binding no longer occurs (*34*).

Proteins in solution experience varying degrees of mobility, which permits the coexistence of various closely related conformations. Conformational changes are a common feature of protein function and protein−protein interactions (*10*, *12*). It has also been suggested recently that less structured and flexible residues of a molecule span a larger conformational space, allowing them to bind to target molecules more quickly (*41*). Observation of relatively broad lines in previous studies of IGF-II by NMR had suggested the possible presence of nonspecific aggregation and/or conformational averaging (*42*). Dual resonant peaks were observed for a number of residues of C-BP-6 in the ^{15}N-^{1}H HSQC spectrum, suggesting their possible involvement in slow conformational/chemical exchange. Moderate line broadening was also evident for C-BP-6 in solution, as reflected in its ^{15}N R_2 values (10.35 ± 3.17 s^{-1}), which are higher than would normally be expected for a 107-residue protein. The experimentally measured translational-diffusion coefficient agrees well with the value calculated from the monomeric NMR structure, implying that C-BP-6 is monomeric in solution. Thus, the observed relatively higher R_2 values might have arisen from conformational/chemical exchange.

While the ^{15}N relaxation studies presented in this paper indicate that C-BP-6 is considerably mobile in solution across a wide range of time scales, it binds IGF-II with micromolar affinity (*34*). Residues of C-BP-6 undergoing conformational exchange showed a good correlation with those that disappeared or broadened upon IGF-II binding, as shown in Figure 6. The peak broadening and disappearance caused by binding to IGF-II was attributed to intermediate exchange between the free and bound forms of C-BP-6 (Headey, S. J., Keizer, D. W., Yao, S., Kantharidis, P., Bach, L. A., and Norton, R. S. (2004) C-terminal domain of insulin-like growth factor binding protein-6: structure and interaction with insulin-like growth factor-II. *Molecular Endocrinology*, accepted for publication.), although an increased contribution of conformational exchange in C-BP-6 cannot be ruled out. A recent study of protein−ligand interaction kinetics by Mittag et al. (*43*) also showed an increased exchange contribution to the ^{15}N transverse relaxation rate in the initial binding steps of a polyoma middle T antigen peptide with N-terminal src homology 2 domain (SH2) of phosphatidylinositide-3-kinase (PI3K). Overall, the correlation observed between residues exhibiting motion at submilli- to millisecond time scales and those involved in IGF-II binding observed in the present study strongly suggests possible conformation switching or population shifting between preexisting conformations in C-BP-6 upon binding to IGF-II. This is also consistent with the observed improvement in the quality of IGF-II spectra in terms of both spectral dispersion and peak line width after binding to full-length IGFBP-2 (at a concentration ratio of 1:1), even though the molecular mass of the complex is much larger than that of the free IGF-II (*44*).

In this paper, we have shown that the C-terminal domain of IGFBP-6 is considerably mobile at time scales ranging from pico- to nanoseconds and that a substantial number of residues in C-BP-6 exhibit conformational exchange at submilli- to millisecond time scales. Importantly, a close correlation between residues exhibiting conformational exchange at submilli- to millisecond time scales and those involved in IGF-II binding is clearly apparent. This observation strongly supports the hypothesis that protein conformational exchange may play an important role in the interactions between IGFBPs and IGFs. Moreover, it will be of great interest to extend this study to full-length IGFBP-6 in the future, because full-length IGFBP-6 binds IGF-II with higher affinity, so that a detailed relaxation study of IGFBP-6 in complex with IGF-II may then become possible.

ACKNOWLEDGMENT

We thank the Cooperative Research Centre for Cellular Growth Factors (Australia) for financial support (S.Y. and R.S.N.), Nigel Parker and Phillip Kantharidis for assistance with C-BP-6 expression and purification, and John Wallace for generously providing us with IGF-II. We also thank Arthur Palmer for helpful discussions.

SUPPORTING INFORMATION AVAILABLE

All ^{15}N relaxation data of C-BP-6 measured in the laboratory and the rotating frames, as well as Modelfree fitting parameters (19 pages). This material is available free of charge via the Internet at http://pubs.acs.org.

REFERENCES

1. Jones, J. I., and Clemmons, D. R. (1995) Insulin-like growth factors and their binding proteins: Biological actions, *Endocr. Rev. 16*, 3−34.
2. Bach L. A. (1999) The insulin-like growth factor system: Basic and clinical aspects, *Aust. N. Z. J. Med. 29*, 355−361.
3. Bach L. A. (1999) Insulin-like growth factor binding protein-6: The "forgotten" binding protein? *Horm. Metab. Res. 31*, 226−234.
4. Baxter, R. C. (2000) Insulin-like growth factor (IGF)-binding proteins: Interactions with IGFs and intrinsic bioactivities, *Am. J. Physiol. Endocrinol. Metab. 278*, 967−976.
5. Kalus, W., Zweckstetter, M., Renner, C., Sanchez, Y., Georgescu, J., Grol, M., Demuth, D., Schumacher, R., Dony, C., Lang, K., and Holak T. A. (1998) Structure of the IGF-binding domain of the insulin-like growth factor-binding protein-5 (IGFBP-5): Implications for IGF and IGF-I receptor interactions, *EMBO J. 17*, 6558−6572.
6. Zeslawski, W., Beisel, H. G., Kamionka, M., Kalus, W., Engh, R. A., Huber, R., Lang, K., and Holak, T. A. (2001) The interaction of insulin-like growth factor-I with the N-terminal domain of IGFBP-5, *EMBO J. 20*, 3638−3644.
7. Palmer, A. G., III (1997) Probing molecular motion by NMR, *Curr. Opin. Struct. Biol. 7*, 732−737.
8. Fischer, M. W. F, Majumdar, A., and Zuiderweg, E. R. P. (1998) Protein NMR relaxation: Theory, applications, and outlook, *Prog. Nucl. Magn. Reson. Spectrosc. 33*, 207−272.
9. Renner, C., and Holak, T. A. (2001) NMR ^{15}N relaxation of the insulin-like growth factor (IGF)-binding domain of IGF binding protein-5 (IGFBP-5) determined free in solution and in complex with IGF-II, *Eur. J. Biochem. 268*, 1058−1065.
10. Feher, V. A., and Cavanagh, J. (1999) Millisecond-timescale motions contribute to the function of the bacterial response regulator protein Spo0F, *Nature 400*, 289−293.
11. Volkman, B. F., Lipson, D., Wemmer, D. E., and Kern, D. (2001) Two-state allosteric behavior in a single-domain signaling protein, *Science 291*, 2429−2433.
12. Frauenfelder, H., Parak, F., and Young, R. D. (1988) Conformational substates in proteins, *Annu. Rev. Biophys. Chem. 17*, 451−479.
13. Headey, S. J., Yao, S., Parker, N. J., Kantharidis, P., Bach, L. A., and Norton, R. S. (2003) ^{1}H, ^{13}C, and ^{15}N resonance assignments of the C-terminal domain of insulin-like growth factor binding protein-6 (IGFBP-6), *J. Biomol. NMR 25*, 251−252.

14. Farrow, N. A., Muhandiram, R., Singer, A. U., Pascal, S. M., Kay, C. M., Gish, G., Shoelson, S. E., Pawson, T., Forman-Kay, J. D., and Kay, L. E. (1994) Backbone dynamics of a free and phosphopeptide-complexed Src homology 2 domain studied by ^{15}N NMR relaxation, *Biochemistry 33*, 5984−6003.
15. Zinn-Justin, S., Berthault, P., Guenneugues, M., and Desvaux, H. (1997) Off-resonance rf fields in heteronuclear NMR: Application to the study of slow motions, *J. Biomol. NMR 10*, 363−372.
16. Mulder, F. A. A., van Tilborg, P. J. A., Kaptein, R., and Boelens, R. (1999) Microsecond time scale dynamics in the RXR DNA-binding domain from a combination of spin-echo and off-resonance rotating frame relaxation measurements, *J. Biomol. NMR 13*, 275−288.
17. Mulder, F. A. A., de Graaf, R., Kaptein, R., and Boelens, R. (1998) An off-resonance rotating frame relaxation experiment for the investigation of macromolecular dynamics using adiabatic rotations, *J. Magn. Reson. 131*, 351−357.
18. Loria, J. P., Rance, M., and Palmer, A. G., III (1999) A relaxation-compensated Carr−Purcell−Meiboom−Gill sequence for characterizing chemical exchange by NMR spectroscopy, *J. Am. Chem. Soc. 121*, 2331−2332.
19. Mulder, F. A. A., Skrynnikov, N. R., Hon, B., Dahlquist, F. W., and Kay, L. E. (2001) Measurement of slow (micros-ms) time scale dynamics in protein side chains by ^{15}N relaxation dispersion NMR spectroscopy: Application to Asn and Gln residues in a cavity mutant of T4 lysozyme, *J. Am. Chem. Soc. 123*, 967−975.
20. Bartels, C., Xia, T., Billeter, M., Güntert, P., and Wüthrich, K. (1995) The program XEASY for computer-supported NMR spectral-analysis of biological macromolecules, *J. Biomol. NMR 6*, 1−10.
21. Kay, L. E., Torchia, D. A., and Bax, A. (1989) Backbone dynamics of proteins as studied by ^{15}N inverse detected heteronuclear NMR spectroscopy−Application to *Staphylococcal* nuclease, *Biochemistry 28*, 8972−8979.
22. Tjandra, N., Feller, S. E., Pastor, R. W., and Bax, A. (1995) Rotational diffusion anisotropy of human ubiquitin from ^{15}N NMR relaxation, *J. Am. Chem. Soc. 117*, 12562−12566.
23. Dosset, P., Hus, J.-C., Blackledge, M., and Marion, D. (2000) Efficient analysis of macromolecular rotational diffusion from heteronuclear relaxation data, *J. Biomol. NMR 16*, 23−28.
24. Mandel, A. M., Akke, M., and Palmer, A. G., III (1995) Backbone dynamics of *Escherichia coli* ribonuclease HI: Correlations with structure and function in an active enzyme, *J. Mol. Biol. 246*, 144−163.
25. Davis, D. G., Perlman, M. E., and London, R. E. (1994) Direct measurements of the dissociation-rate constant for inhibitor-enzyme complexes via the $T_{1\rho}$ and T_2 (CPMG) methods, *J. Magn. Reson. B104*, 266−275.
26. Hwang, T.-L., van Zijl, P. C. M., and Mori, S. (1998) Accurate quantitation of water-amide proton exchange rates using the phase-modulated CLEAN chemical EXchange (CLEANEX-PM) approach with a Fast-HSQC (FHSQC) detection scheme, *J. Biomol. NMR 11*, 221−226.
27. Berman, H. M., Westbrook, J., Feng, Z., Gilliland, G., Bhat, T. N., Weissig, H., Shindyalov, I. N., and Bourne, P. E. (2000) The Protein Data Bank, *Nucleic Acids Res. 28*, 235−242.
28. García de la Torre, J., Huertas, M. L., and Carrasco, B. (2000) HYDRONMR: Prediction of NMR relaxation of globular proteins from atomic-level structures and hydrodynamic calculations, *J. Magn. Reson. 147*, 138−146.
29. Yao, S., Howlett, G. J., and Norton, R. S. (2000) Peptide self-association in aqueous trifluoroethanol monitored by pulsed field gradient NMR diffusion measurements, *J Biomol. NMR 16*, 109−119.
30. Korzhnev, D. M., Tischenko, E. V., and Arseniev, A. S. (2000) Off-resonance effects in ^{15}N T_2 CPMG measurements, *J. Biomol. NMR 17*, 231−237.
31. Yao, S., Hinds, M. G., and Norton, R. S. (1998) Improved estimation of protein rotational correlation times from ^{15}N relaxation measurements, *J. Magn. Reson. 131*, 347−350.
32. Blackledge, M., Cordier, F., Dosset, P., and Marion, D. (1998) Precision and uncertainty in the characterization of anisotropic rotational diffusion by ^{15}N relaxation, *J. Am. Chem. Soc. 120*, 4538−4539.
33. Phan, I. Q. H., Boyd, J., and Campbell, I. D. (1996) Dynamic studies of a fibronectin type I module pair at three frequencies: Anisotropic modeling and direct determination of conformational exchange, *J. Biomol. NMR 8*, 369−378.
34. Headey, S. J., Keizer, D. W., Yao, S., Wallace, J. C., Bach, L. A., and Norton, R. S. (2004) Binding site for the C-domain of insulin-like growth factor (IGF) binding protein-6 on IGF−II; implications for inhibition of IGF actions, *FEBS Letters*, *568*, 19−22.
35. Banci, L., Felli, I. C., and Koulougliotis, D. (1998) Identification of slow motions in the reduced recombinant high-potential iron sulfur protein I (HiPIP I) from *Ectothiorhodospira halophila* via ^{15}N rotating-frame NMR relaxation measurements, *J. Biomol. NMR 12*, 307−318.
36. Barker, P. D., Bertini, I., Conte, R. D., Ferguson, S. J., Hajieva, P., Tomlinson, E., Turano, P., and Viezzoli, S. (2001) A further clue to understanding the mobility of mitochondrial yeast cytochrome *c*: A ^{15}N $T_{1\rho}$ investigation of the oxidized and reduced species, *Eur. J. Biochem. 268*, 4468−4476.
37. Yao, S., Smith, D. K., Hinds, M. G., Zhang, J. -G., Nicola, N. A., and Norton, R. S. (2000) Backbone dynamics measurements on leukemia inhibitory factor, a rigid four-helical bundle cytokine, *Protein Sci. 9*, 671−682.
38. Pawley, N. H., Wang, C., Koide, S., and Nicholson, L. K. (2001) An improved method for distinguishing between anisotropic tumbling and chemical exchange in analysis of ^{15}N relaxation parameters, *J. Biomol. NMR 20*, 149−165.
39. Campos-Olivas, R., and Summers, M. F. (1999) Backbone dynamics of the N-terminal domain of the HIV-1 capsid protein and comparison with the G94D mutant conferring cyclosporin resistance/dependence, *Biochemistry 38*, 10262−10271.
40. Millet, O., Loria, J. P., Kroenke, C. D., Pons, M., and Palmer, A. G., III (2000) The static magnetic field dependence of chemical exchange linebroadening defines the NMR chemical shift time scale, *J. Am. Chem. Soc. 122*, 2867−2877.
41. Duggan, B. M., Dyson, H. J., and Wright, P. E. (1999) Inherent flexibility in a potent inhibitor of blood coagulation, recombinant nematode anticoagulant protein c2, *Eur. J. Biochem. 265*, 539−548.
42. Torres, A. M., Forbes, B. E., Aplin, S. E., Wallace, J. C., Francis, G. L., and Norton, R. S. (1995) Solution structure of human insulin-like growth factor II. Relationship to receptor and binding protein interactions, *J. Mol. Biol. 248*, 385−401.
43. Mittag, T., Schaffhausen, B., and Günther, U. L. (2003) Direct observation of protein−ligand interaction kinetics, *Biochemistry 42*, 11128−11136.
44. Carrick, F. E. (2001) *Characterization of Bovine Insulin-Like Growth Factor Binding Protein-2: Structure and Function*, Ph.D. Thesis, Adelaide University, Adelaide, Australia.
45. Koradi, R., Billeter, M., and Wüthrich, K. (1996) MOLMOL: A program for display and analysis of macromolecular structures, *J. Mol. Graphics 14*, 51−55.

BI049456+